The 8th European Congress on Computational Methods in Applied Sciences and Engineering
ECCOMAS Congress 2022
5–9 June 2022, Oslo, Norway

AN IMMERSED BOUNDARY METHOD FOR THE CFD SOLVER AIRBUS-CODA

VÍCTOR J. LLORENTE[1,2], DIEGO LODARES[1,3], ESTEBAN FERRER[1,2] AND EUSEBIO VALERO[1,2]

[1] ETSIAE-UPM - School of Aeronautics
Universidad Politécnica de Madrid
Plaza Cardenal Cisneros 3, E-28040 Madrid, Spain
e-mail: victorjavier.llorente@upm.es, d.lodares@alumnos.upm.es, esteban.ferrer@upm.es, eusebio.valero@upm.es

[2] Center for Computational Simulation
Universidad Politécnica de Madrid
Campus de Montegancedo, Boadilla del Monte, 28660, Madrid, Spain
e-mail: victorjavier.llorente@upm.es, esteban.ferrer@upm.es, eusebio.valero@upm.es

[3] Airbus Defence and Space
Avenida de John Lennon s/n, 28906 Getafe, Spain
email: diego.lodares@airbus.com

Key words: Immersed Boundary Method, Volume Penalization, CODA

Abstract. This work implements and analyses an Immersed Boundary Method based on Volume Pezalization for the flow simulator Airbus-CODA (**C**FD for **O**NERA, **D**LR, and **A**IRBUS). The Immersed Boundary Volume Penalization has unique advantages, e.g. easy to implement, straightforward formulation for moving geometries, and numerical errors can be controlled a-priori [1, 2], showing the potential for aeronautical applications. Numerical experiments will assess the accuracy of the Immersed Boundary Volume Penalization in CODA.

1 INTRODUCTION

1.1 Immsered Boundary Volume Penalization

The Immersed Boundary Method (IBM) [3] is a popular numerical approach to mimic the effect of boundary conditions in the flow without requiring body-fitted meshes. IBM reduce considerably the effort of mesh generation and can easily handle moving geometries. In general, the IBM can be achieved by the cut-cell approach [4], by the introduction of source terms such as the ghost cell [5, 6], direct forcing [7] or volume penalisation, among others, or by interface modification [8, 9].

Volume Penalization (VP) [10, 11, 12, 13] belongs to that class of IBM where the governing equations (i.e. the compressible Navier-Stokes (NS) equations),

$$\frac{\partial \boldsymbol{\phi}}{\partial t} + \nabla \cdot \mathbf{F} = \mathbf{s}_\eta, \tag{1}$$

are penalized to drive the flow velocity to specied values (e.g. zero in stationary geometries) in grid nodes representing the body. The boundary condition are imposed by introducing a source term or penalty term,

$$\mathbf{s}_\eta = -\frac{\chi}{\eta}\begin{pmatrix} 0 \\ \rho\left[\mathbf{u}-\mathbf{u}_s\right] \\ \dfrac{\rho}{2}\left[\mathbf{u}\cdot\mathbf{u}-\mathbf{u}_s\cdot\mathbf{u}_s\right] \end{pmatrix} \tag{2}$$

to the computational nodes located inside the body. The conservative variable vector and the total fluxes are respectively,

$$\boldsymbol{\phi} = \begin{pmatrix} \rho \\ \rho\mathbf{u} \\ \rho e \end{pmatrix}, \quad \mathbf{F} = \begin{pmatrix} \rho\mathbf{u} \\ \rho\mathbf{u}\otimes\mathbf{u}+p\mathbf{I}-\mathbf{E} \\ \left[\rho e+p\right]\mathbf{u}-\mathbf{E}\mathbf{u}-\mathbf{q} \end{pmatrix}, \tag{3}$$

with thermodinamics variables such as the static pressure, $p = [\gamma - 1]\rho T$, and temperature, $c_v T = e - \mathbf{u}\cdot\mathbf{u}/2$. Viscous stress tensor and heat flux are respectively,

$$\mathbf{E} = \mu\left[\nabla\mathbf{u} + (\nabla\mathbf{u})^{\mathrm{T}} - \frac{2}{3}\left[\nabla\cdot\mathbf{u}\right]\mathbf{I}\right], \quad \mathbf{q} = -\kappa\nabla T. \tag{4}$$

In the above equations ρ is the density, $\mathbf{u}$ is the velocity vector, e is the total energy, γ is the specific hear ratio, c_v is the specific heat at constant volume, μ is the dinamic viscosity, $0 < \eta \ll 1$ is the penalization parameter, and $\mathbf{u}_s$ is the solid velocity vector. The mask function, χ, which distinguishes between the fluid, Ω_{f}, and body, Ω_{b}, regions, can be defined as

$$\chi = \begin{cases} 1, & \text{If } \mathbf{x} \in \Omega_{\mathrm{b}} \\ 0, & \text{Otherwise} \end{cases}, \tag{5}$$

and is called *sharp*. Kolomenskiy and Schneider [14] point out another formulation to avoid spurious oscillations of the hydrodynamic forces by smoothing the mask function. Following [11], the *smooth* mask function can be defined as

$$\chi = \left[1 - \exp\left(-\left(||\mathbf{x}-\mathbf{x}_{\mathrm{w}}||_2/\delta\right)^2\right)\right]\chi_{\mathrm{sharp}}, \tag{6}$$

where $||\mathbf{x}-\mathbf{x}_{\mathrm{w}}||_2$ is the Euclidean distance to the wall and δ is the width of the smoothing function.

1.2 Mask function with triangular surface

Working with industrial (or academic) CFD aerodynamics solvers, the body geometry is usually given in an STL file [15]. Now the body is represented by triangular surfaces given by a cloud of points $\{x_i, y_i, z_i\}$ $i = 0, \ldots, n-1$. To answer if a computational node lives inside the body, ones start by checking whether it is inside an Oriented Bounding Box (OBB) around the body, following Mukundan [16].

An OBB is the minimal cuboid that encloses a set of points in space (i.e., the triangular points of the STL file). The procedure begins by calculating the centroid of the body, $(\overline{x}, \overline{y}, \overline{z})$, and defining the matrix,

$$\mathbf{V} = \begin{pmatrix} x_0 - \overline{x} & x_1 - \overline{x} & \dots & x_{n-1} - \overline{x} \\ y_0 - \overline{y} & y_2 - \overline{y} & \dots & y_{n-1} - \overline{y} \\ y_0 - \overline{z} & z_3 - \overline{z} & \dots & z_{n-1} - \overline{z} \end{pmatrix} \in \mathbb{R}^{3\times n} \tag{7}$$

and the covariance matrix (symmetric),

$$\mathbf{C} = \frac{1}{n}\left(\mathbf{V}\mathbf{V}^{\mathrm{T}}\right) \in \mathbb{R}^{3\times 3} \tag{8}$$

The principal directions of $\mathbf{C}$ are then determined to orient the faces of the OBB and the eigenvalues, $\{\lambda_1, \lambda_2, \lambda_3\}$, of $\mathbf{C}$ to give the half-width of the OBB face, $\{w_j = \sqrt{\lambda_j}\}$ $j = 1, 2, 3$. Finally the two-dimensional rotating calipers method applies over their projections onto the plane that is normal to the direction with the smallest associated eigenvalue.

If a computational node tests positive within the OBB, a second test is necessary to determine if it is actually within the triangular surface. In order to do this, ones calculate signed distances from the positive computational node towards surface projections, along vertical rays, defining the vertical direction as the longest axis of the OBB.

2 NUMERICAL RESULTS

The implementation of the Immersed Boundary Volume Penalization (IBVP) previously described is performed in the 3D solver CODA [17]. For spatial discretization, a second-order cell-centered finite volume is used. Convective and diffusion fluxes are computed by the Roe-upwinding and central schemes respectively. For temporal discretization, an implicit Euler scheme with Switched Evolution Relaxation (SER) method [18] are used. The implicit scheme allows for the penalty η to be arbitrarily high, enabling precision when imposing the IB.

2.1 Analysis

The solver is validated by simulating steady and unsteady flow past a cylinder with diameter D immersed in an uniform Cartesion mesh. Simulations have been performed in a $[-5D, 15D] \times [-D/2, D/2] \times [-5D, 5D]$ domain with $200 \times 1 \times 160$ nodes. The IBVP was configured with a it sharp mask function. Flow field is plotted in Figure 1a with Reynolds number $Re = 40$ at low Mach number of $Ma = 0.2$. The Reynolds number is defined by the cylinder diameter D and the freestream velocity U_∞, (i.e. $Re \coloneqq \rho U_\infty D/\mu$). It is observed the momentum in x direction, Figure 1b, drops zero within the origin because is in this region of the domain where the penalty body force works driving the velocity of the fluid to zero.

Keeping the Reynolds number, a second test comprises an analysis where the change in the flow field is evaluated upon the variation of the penalization parameter, see Figure 2. Smaller the volume penalization parameter, the IBVP mimics a NS flow around a cylinder. Less than a value of 10^{-5} it needs to set a smaller initial CFL number.

The implementation of a *smooth* mask function is plotted in FIgure 3. Bigger the value of δ, bigger the zone of the of the zone of the penalization of the IBVP and smaller the initial CFL number. In the simulations that were run with this mask function (and is not plotted here), it was observed that a not right choice of values for the set $\{\eta,\ \delta,\ \mathrm{CFL}_{\mathrm{ini}}\}$, turns the conservative variable vector into negative.

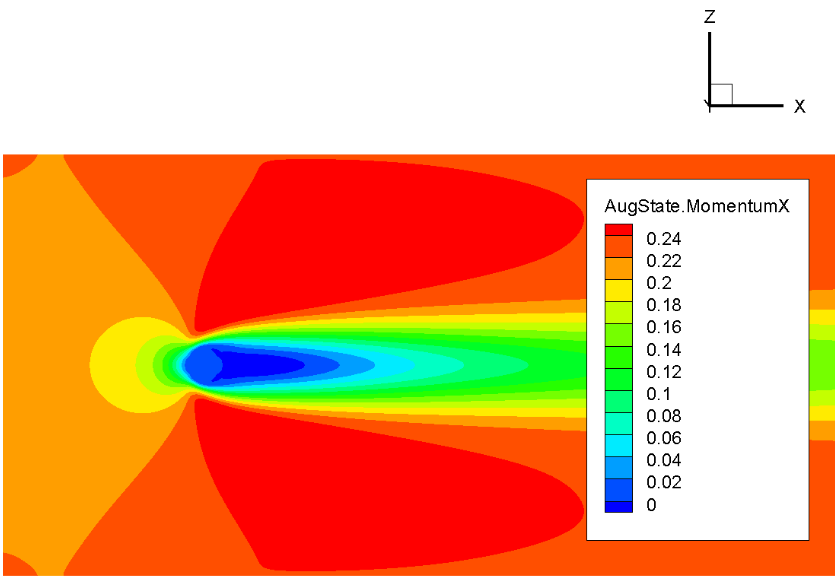

(a) Flow field.

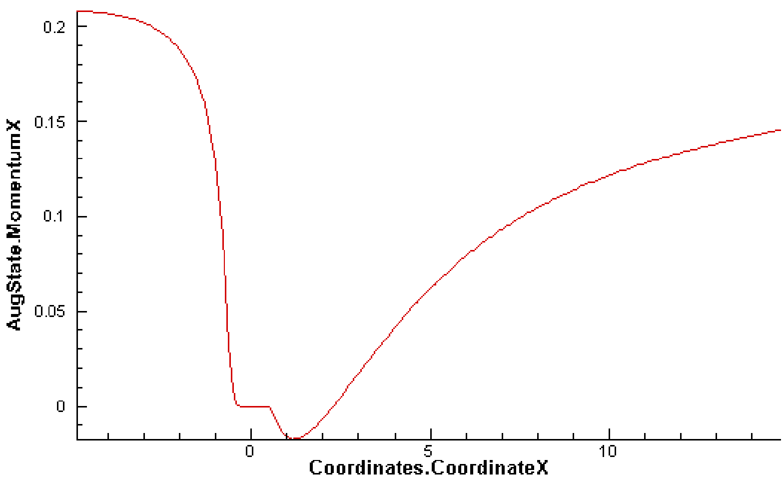

(b) x-Momentum along the line $z = 0$.

Figure 1: IBVP simulation around a cylinder.

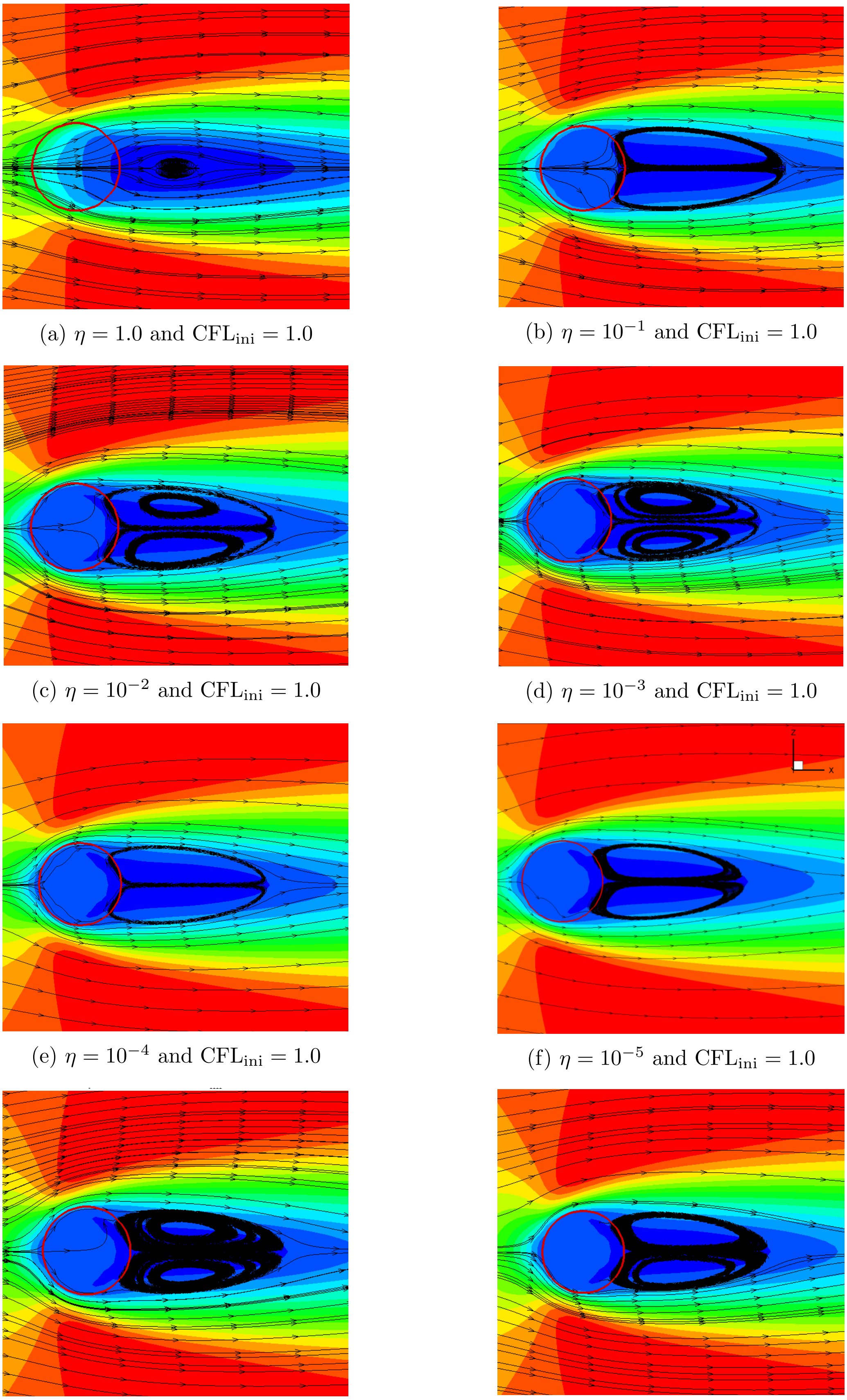

(a) $\eta = 1.0$ and $\mathrm{CFL}_{\mathrm{ini}} = 1.0$

(b) $\eta = 10^{-1}$ and $\mathrm{CFL}_{\mathrm{ini}} = 1.0$

(c) $\eta = 10^{-2}$ and $\mathrm{CFL}_{\mathrm{ini}} = 1.0$

(d) $\eta = 10^{-3}$ and $\mathrm{CFL}_{\mathrm{ini}} = 1.0$

(e) $\eta = 10^{-4}$ and $\mathrm{CFL}_{\mathrm{ini}} = 1.0$

(f) $\eta = 10^{-5}$ and $\mathrm{CFL}_{\mathrm{ini}} = 1.0$

(g) $\eta = 10^{-6}$ and $\mathrm{CFL}_{\mathrm{ini}} = 2 \cdot 10^{-2}$

(h) $\eta = 10^{-7}$ and $\mathrm{CFL}_{\mathrm{ini}} = 2 \cdot 10^{-3}$

Figure 2: Flow filed for differents values of penalization parameter. The red circle represents the immersed cylinder.

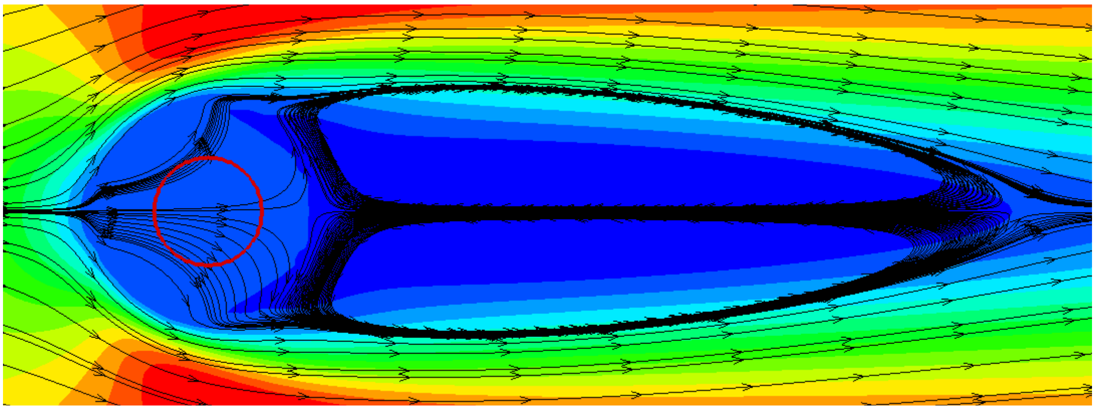

(a) $\eta = 10^{-1}$, $\delta = 10^{-1}$, and $\mathrm{CFL_{ini}} = 10^{-2}$

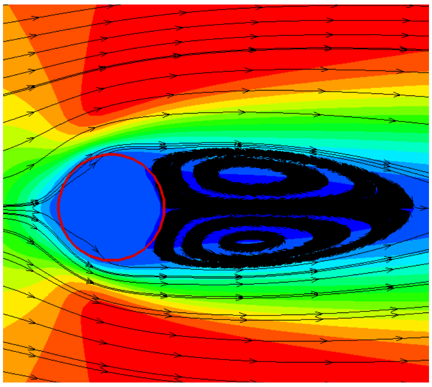

(b) $\eta = 10^{-1}$, $\delta = 10^{-2}$, and $\mathrm{CFL_{ini}} = 1.0$

Figure 3: Simulations with a *smooth* mask function. The red circle represents the immersed cylinder.

Comparisons with other experimental and computational results of the length of recirculation are tabulated in Tables 1, 2, and 3. The third column of the tables is the relative error with respect to the body-fitted result. It is found that the IBVP with a *sharp* mask function the results are comparable with other numerical simulations and experiments. The length of recirculation for the IBVP with *smooth* mask function is bigger than other numerical results because δ is not enough smaller.

Table 1: Length of recirculation for a cylinder at $Re = 40$ reported in the literature. (E) stands for experimental; (body-fitted) and (IBM), numerical.

Study	L_{rb}/D	|rel. error| [%]
Cuntanceau & Bouard [19][(E)]	1.89	
Fornberg [20][(body-fitted)]	2.24	—
Ye *et al.* [4][(IBM)]	2.27	1.33(9)
Choi *et al.* [7][(IBM)]	2.21	1.33(9)
Brehm *et al.* [9][(IBM)]	2.26	0.89(3)

Table 2: Length of recirculation for a cylinder at $Re = 40$ computed with a *sharp* mask function.

Present study - sharp	L_{rb}/D	|rel. error| [%]
$\eta = 10^{-7}$	2.21	1.33(9)
$\eta = 10^{-6}$	2.27	1.33(9)
$\eta = 10^{-5}$	2.29	2.23(2)
$\eta = 10^{-4}$	2.28	1.78(6)
$\eta = 10^{-3}$	2.27	1.33(9)
$\eta = 10^{-2}$	2.28	1.78(6)
$\eta = 10^{-1}$	2.37	5.80(4)

Finally, an unsteady simulation was performanced with $Re = 100$ and $Ma = 0.2$, see Figure 4. The computation of the Strouhal number ($St \coloneqq fD/U_\infty$), quantity that characterizes the shedding frequency of vortex f, is compared with experimental and numerical results reported in the literature in Table 4. Here St has been estimated from the frequency taken by a vortex going from point "A" to point "B". Results similar to those of the literature are found.

2.2 Applications

To see the potencial of IBVP and the implementation of the mask function. In the first case a oscillating cylinder was performanced at $Re = 40$. The motion is expressed as $z(t) = A_m \sin(\pi/2 f_m t)$, where A_m and f_m are the amplitude and frecuency of the oscillating motion. The computational domain is the same as previous simulations but the mesh is set to $800\times1\times400$. The flow past around the moving cylinder is in Figure 5. In each iteration the code is able to

Table 3: Length of recirculation for a cylinder at $Re = 40$ computed with a *smooth* mask function with $\delta = 10^{-2}$.

Present study - smooth	L_{rb}/D	|rel. error| [%]
$\eta = 10^{-7}$	2.77	23.66(1)
$\eta = 10^{-6}$	2.78	24.10(7)
$\eta = 10^{-5}$	2.77	23.66(1)
$\eta = 10^{-4}$	2.77	23.66(1)
$\eta = 10^{-3}$	2.78	24.10(7)
$\eta = 10^{-2}$	2.79	24.55(4)
$\eta = 10^{-1}$	2.85	27.23(2)

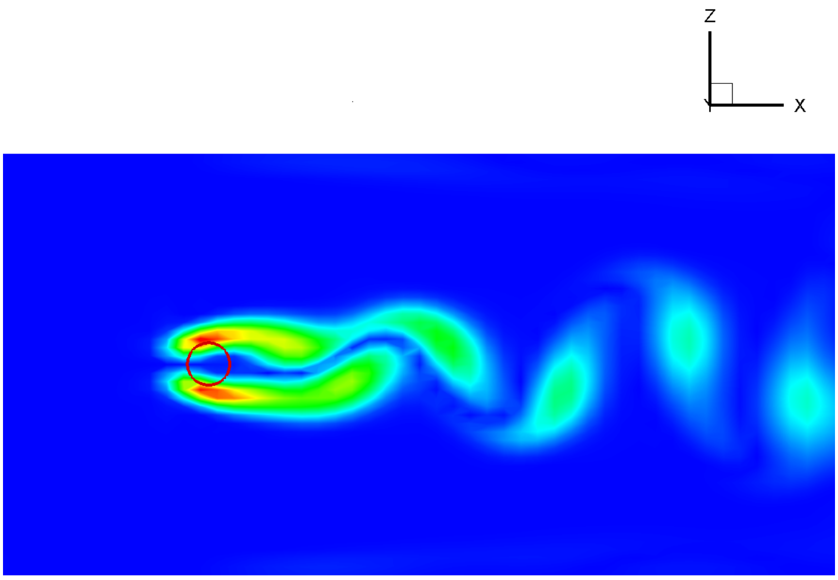

Figure 4: Vorticity magnitude at $Re = 100$. The red circle represents the immersed cylinder.

Table 4: Comparison of result for $Re = 100$ considering the Strouhal number (St). (E) stands for experimental; (body-fitted) and (IBM), numerical.

Study	St
Williamson [21](E)	0.161
Fet *et al.* [22](E)	0.165
Roshko [23](E)	0.167
Zhang *et al.* [24](body-fitted)	0.172
Mittal *et al.* [6](IBM)	0.166
Present study - sharp $\eta = 10^{-5}$	0.154

update the mask function without modify the mesh. A second case was performanced with an Airbus XRF1 wing in a computational domain $[0, 60] \times [0, 40] \times [0, 3]$ and a mesh $200 \times 100 \times 160$, see Figure 6. The geometry is given in a STL file with 13k elements. The time request to generate the mesh was around 4.3 min.

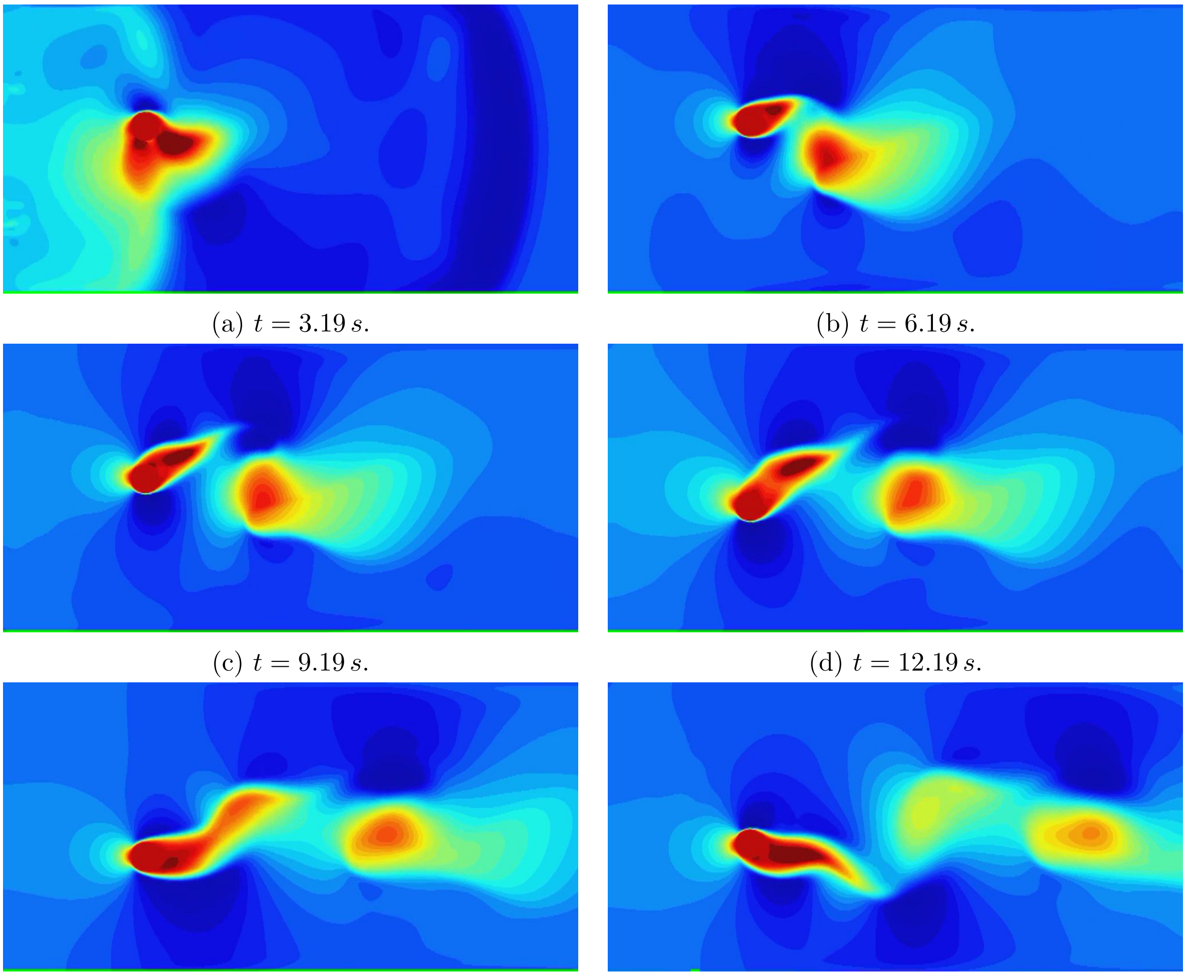

(a) $t = 3.19\,s$. (b) $t = 6.19\,s$. (c) $t = 9.19\,s$. (d) $t = 12.19\,s$. (e) $t = 15.19\,s$. (f) $t = 18.19\,s$.

Figure 5: Moving boundary problem.

3 CONCLUSIONS

An Immersed Boundary Volumen Penalization (IBVP) is implimented in the Airbus-CODA solver. The mask function can deal with STL files. An analysis of the IBVP founds results in concordance with other Immersed Boundary Method (IBM) families. The *sharp* mask function seems to be a good approach for an immersed body and we do not observe improvements when using the non-*sharp* mask. Further study should be done, e.g. a von Neumann stability analysis, for the *smooth* mask function to find the optimal values and determine when the *smooth* mask

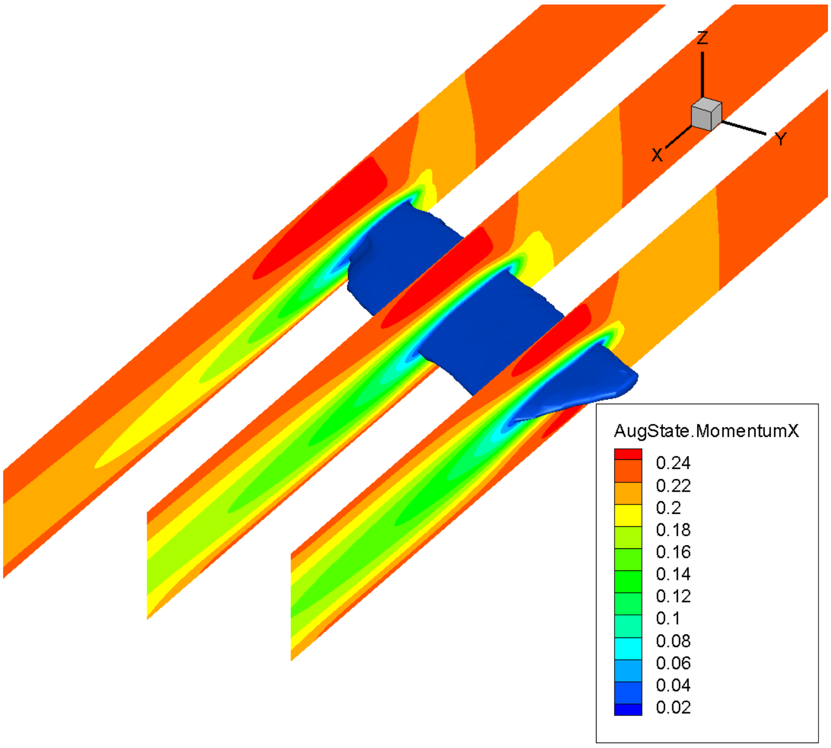

Figure 6: Fluid flow around a wing in a laminar regimen. The blue isosurface represents the region of the domain where momentum drops near zero.

is comparable to the *sharp* one. The IBM provides flexibility for static and moving geometries and will be further extended to simulate aircraft configurations in CODA.

ACKNOWLEDGEMENTS

VJL, EF, and EV acknowledge the finantial support of the European High-Performance Computing Joint Undertaking (JU) under grant agreement (No 956104). The JU receives support from the European Union's Horizon 2020 research and innovation programme under grant agreement (No 823844) and Spain, France, Germany. CODA is the computational fluid dynamics (CFD) software being developed as part of a collaboration between the French Aerospace Lab ONERA, the German Aerospace Center (DLR), Airbus, and their European research partners. CODA is jointly owned by ONERA, DLR and Airbus.

REFERENCES

[1] Brown-Dymkoski, E., Kasimov, N. and Vasilyev, O.V. A characteristic based volume penalization method for general evolution problems applied to compressible viscous flows. *Journal of Computational Physics* (2014) **262**:344-–357.

[2] Kou, J., Llorente, V.J., Valero, E., Ferrer, E. A Modified Equation Analysis for Immersed Boundary Methods based on Volume Penalization: Applications to Linear Advection-Diffusion and High-Order Discontinuous Galerkin Schemes. *Under review at Journal of Scientific Computing.*

[3] Mittal, R. and Iaccarino G. Immersed Boundary Methods. *Annual Review of Fluid Mechanics* (2005) **37**:239–261.

[4] Ye, T., Mittal, R., Udaykumar, H.S. and Shyy, W. An accurate Cartesian Grid Method for Viscous Incompressible Flows with Complex Immersed Boundaries. *Journal of Computational Physics* (1999) **156**:209–240.

[5] Majumdar, S., Iaccarino, G. and Durbin, PA. RANS solver with adaptive structured boundary non-conforming grids. *Annual Research Briefs 2001, Center for Turbulence Research* (2001):353-–366.

[6] Mittal, R., Dong, H., Bozkurttas, M., Najjar, F.M., Vargas, A. and von Loebbecke, A. A versatile sharp interface immersed boundary method for incompressible flows with complex boundaries. *Journal of Computational Physics* (2008) **227**:4825—4852.

[7] Choi, J.-I., Oberoi, R.C., Edwards, J.R. and Rosati, J.A. An immersed boundary method for complex incompressible flows. *Journal of Computational Physics* (2007) **224**:757-–784.

[8] Brahmachary, S., Natarajan, G., Kulkarni, V., Sahoo, N., Ashok, V. and Kumar V. Role of solution reconstruction in hypersonic viscous computations using a sharp interface immersed boundary method. *Physical Review E* (2021) **103**:043302.

[9] Brehm, C., Hader, C. and Fasel, H.F. A locally stabilized immersed boundary method for the compressible Navier-Stokes equations. *Journal of Computational Physics* (2015) **295**:475-–504.

[10] Kou, J., Hurtado-de-Mendoza, A., Joshi, S., Le Clainche, S., and Ferrer, E. Eigensolution analysis of immersed boundary method based on volume penalization: applications to high-order schemes. *Journal of Computational Physics* (2022) **449**:110817.

[11] Kou, J., Joshi, S., Hurtado-de-Mendoza, A., Puri, K., Hirsch, C. and Ferrer E. Immersed boundary method for high-order flux reconstruction based on volumen penalization. *Journal of Computational Physics* (2022) **448**:110721.

[12] Kou, J. and Ferrer E. A combined volume penalization / selective frequency damping for immersed boundary methods applied to high-order schemes. *Under review at Journal of Computational Physics.*

[13] Abalakin, I.V., Zhdanova, N.S. and Kozubskaya T.K. Immersed boundary method implemented for the simulation of an external flow on unstructured meshes. *Mathematical Models and Computer Simulations* (2016) **8**:219-–230.

[14] Kolomenskiy, D. and Schneider, K. A Fourier spectral method for the Navier–Stokes equations with volume penalization for moving solid obstacles. *Journal of Computational Physics* (2009) **228**:5687–5709.

[15] Szilvśi-Nagygy, M. and Mátyási Gy. Analysis of STL files. *Mathematical and Computer Modelling* (2003) **38**(7-9):945–960.

[16] Mukundan, R. *Advanced Methods in Computers Graphics: with examples in OpenGL.* Springer (2012).

[17] Wagner, M. The CFD Solver CODA and the Sparse Linear Systems Solver Spliss: Evaluation of Performance and Scalability. *NHR CFD Workshop Day 2021.*

[18] Mulder, W. and van Leer, B. Experiments with implicit upwind methods for the Euler equations. *Journal of Computational Physics* (1985) **59**:232–246.

[19] Cuntanceau, M. and Bouard, R. Experimental determination of the main features of the viscous flow in the wake of a circular cylinder in uniform translation. Part 1. Steady flow. *Journal of Fluid Mechanics* (1973) **79**:257-–272.

[20] Fornberg, B. A numerical study of steady viscous flow past a circular cylinder. *Journal of Fluid Mechanics* (1980) **98**:819-–855.

[21] Williamson, C.H.K. The natural and forced formation of spot-like' vortex dislocations' in the transition of a wake. *Journal of Fluid Mechanics* (1992) **243**:393-–441.

[22] Fet, U., König, M. and Eckelmann, H. A new Strouhal-Reynolds-number relationship for the circular cylinder in the range $47 < Re < 23 \cdot 10^5$. *Physics of Fluids* (1998) **10**:1547.

[23] Roshko, A. On the Development of Turbulent Wakes from Vortex Streets. *Washington, DC, NACA Report 1191, National Advisory Committee for Aeronautics* (1954).

[24] Zhang, H.-Q., Fey, U., Noack, B.R., König, M. and Eckelmann, H. On the transition of the cylinder wake. *Physics of Fluids* (1995) **7**:779.